Title: Duffy Antigen is Expressed During Erythropoiesis in Duffy Negative Individuals

Running Title: Duffy Antigen Expression in Duffy Negative Individuals

Celia Dechavanne[1,10], Sebastien Dechavanne[1,10], Jürgen Bosch[1,2,10], Sylvain Metral[3], Karli R. Redinger[1], Quentin D. Watson[1], Arsene, C. Ratsimbasoa[4,5], Brooke Roeper[1], Sushma Krishnan[1], Rich Fong[1], Seth Bennett[1], Lenore Carias[1], Edwin Chen[6], Nichole D. Salinas[7], Anil Ghosh[1], Niraj H. Tolia[7], Philip G. Woost[8], James W. Jacobberger[8], Yves Colin[3], Benoit Gamain[3,*], Christopher L. King[1,9,*], Peter A. Zimmerman[1,11,*].

Supplemental Information

1. Study Participants

Table S1. Study Donor Information related to all figures.

ID	Tissue	Sample	Sex	Age	Genotype	Phenotype
#1	Peripheral Blood	D2	F	21	*FY*B ^{ES} /*B ^{ES}*	Fya-b-
#2	Peripheral Blood	D3	F	21	*FY*B ^{ES} /*B ^{ES}*	Fya-b-
#3	Peripheral Blood	BB	M	38	*FY*B/*B*	Fya-b+
#4	Peripheral Blood	AB	F	36	*FY*A/*B*	Fya+b+
#5	Peripheral Blood	AA	M	27	*FY*A/*A*	Fya+b-
#6	Bone Marrow	BM_863	M	62	*FY*B ^{ES} /*B ^{ES}*	Fya-b-
#7	Bone Marrow	BM_864	M	41	*FY*B ^{ES} /*B ^{ES}*	Fya-b-
#8	Bone Marrow	BM_874	M	37	*FY*B ^{ES} /*B ^{ES}*	Fya-b-
#9	Bone Marrow	BM_766	F	39	*FY*B ^{ES} /*B ^{ES}*	Fya-b-
#10	Bone Marrow	BM_885	F	35	*FY*A/*B*	Fya+b+
#11	Bone Marrow	BM_786	M	31	*FY*B/*B*	Fya-b+
#12	Bone Marrow	BM_797	M	31	*FY*A/*B ^{ES}*	Fya+b-
#13	Bone Marrow	BM_838	M	62	*FY*A/*B ^{ES}*	Fya+b-
#14	Bone Marrow	BM_881	F	37	*FY*B/*B ^{ES}*	Fya-b+
#15	Bone Marrow	BM_875	M	33	*FY*A/*B ^{ES}*	Fya+b-
#16	Bone Marrow	BM_735	M	45	*FY*A/*B ^{ES}*	Fya+b-
#17	Bone Marrow	BM_565	M	40	*FY*A/*B*	Fya+b+
#18	Frozen RBC	36253	M	na	*FY*B ^{ES} /*B ^{ES}*	Fya-b-
#19	Frozen RBC	5873	F	na	*FY*B ^{ES} /*B ^{ES}*	Fya-b-
#20	Frozen RBC	31395	M	na	*FY*B ^{ES} /*B ^{ES}*	Fya-b-
#21	Frozen RBC	20636	M	na	*FY*B ^{ES} /*B ^{ES}*	Fya-b-
#22	Frozen RBC	12725	F	na	*FY*B ^{ES} /*B ^{ES}*	Fya-b-
#23	Frozen RBC	12664	F	na	*FY*B ^{ES} /*B ^{ES}*	Fya-b-
#24	Frozen RBC	39207	F	na	*FY*B ^{ES} /*B ^{ES}*	Fya-b-
#25	Frozen RBC	6293	M	na	*FY*B ^{ES} /*B ^{ES}*	Fya-b-
#26	Frozen RBC	21667	F	na	*FY*B ^{ES} /*B ^{ES}*	Fya-b-
#27	Frozen RBC	24947	F	na	*FY*B ^{ES} /*B ^{ES}*	Fya-b-
#28	Peripheral Blood	RO	M	28	*FY*B ^{ES} /*B ^{ES}*	Fya-b-
#29	Peripheral Blood	JB	M	47	*FY*B /*B ^{ES}*	Fya-b+
#30	Peripheral Blood	RT	M	25	*FY*A/*B*	Fya+b+

2. CA111 specificity and affinity for Fy protein

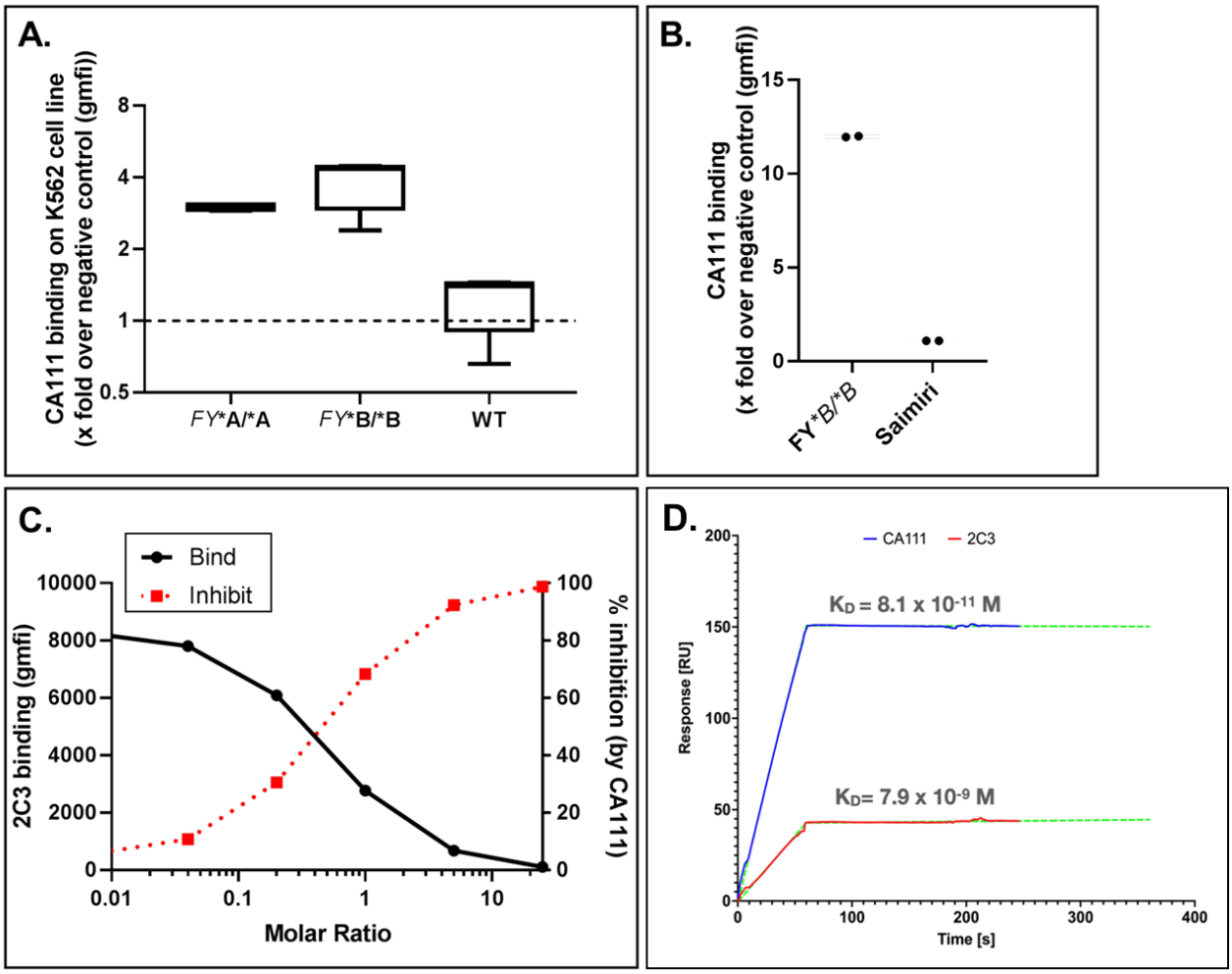

Figure S1. Binding of CA111 to Fy expressing cells only, competition with 2C3 and affinity for the Fy protein related to Figure 1.

Panel S1A. CA111 binding was performed on not transfected K562 cell line (Wild Type (WT), N=3) and the *FY*A/*A* (N=3) or *FY*B/*B* (N=3) transfected K562.

Panel S1B. CA111 binding was performed on *FY*B/*B* and Saimiri pbRBC. As expected, no signal was observed on Saimiri pbRBC compared to *FY*B/*B*.

Panel S1C. Inhibition of 2C3 binding by the CA111. Because the 2C3 and the CA111 are binding to the same epitope on the Fy protein ([22]**FEDVW**[26]), a competition assay between the 2 antibodies was performed. RBCs were pre-incubated with increasing concentrations of CA111 (molar ratio

from 0 to 25) an hour at 37°C. 2C3 was then directly added (no wash) at 5 µg/mL.

Panel S1D. SPR analysis of the binding between DARC and CA111 or 2C3. nDARC is immobilized to an SPR chip and passing either CA111 or 2C3 over the surface to determine the binding constants. Our results confirmed the K_D that Smolareck *et al* have previously published [S1] and showed a better affinity of CA111 to nDARC than the 2C3 antibody.

3. Erythrocyte binding assays

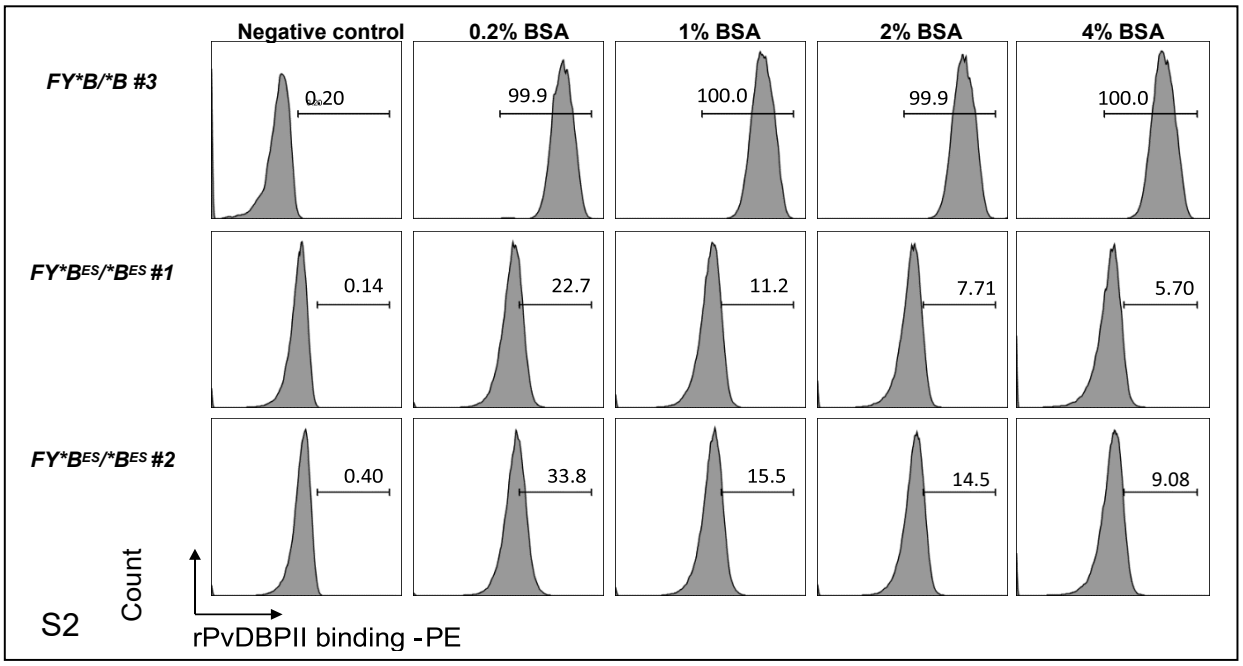

Figure S2. The effect of increasing BSA concentration on rPvDBPII binding to peripheral blood RBC (pbRBC) from Fy-positive and Fy-negative donors related to Figure 1.

The rationale for this experiment was to determine if the signal of rPvDBPII was persisting after elimination of non-specific binding to donor pbRBC with increasing BSA concentrations during pre-incubation steps in erythrocyte binding assays; particular interest was focused on the results for *FY*B^{ES}/*B^{ES}* (donors #1 and #2). The binding of rPvDBPII to pbRBC was monitored by flow cytometry by comparing rPvDBPII-specific fluorescence of negative controls (minus rPvDBPII; plus secondary anti-rPvDBPII, rabbit polyclonal antibody; plus anti-rabbit phycoerythrin- conjugateted goat antibody) to rPvDBPII-specific fluorescence at increasing BSA concentrations (0.2%1.0%, 2.0% and 4.0%). The percentage of positive cells for rPvDBPII binding of each individual pbRBC

donor is indicated above the gate determined for positive rPvDBPII binding.

4. **Binding competition of CA111 in the presence of nDARC to *FY*B/*B* and *FY*B^{ES}/*B^{ES}* red cells**

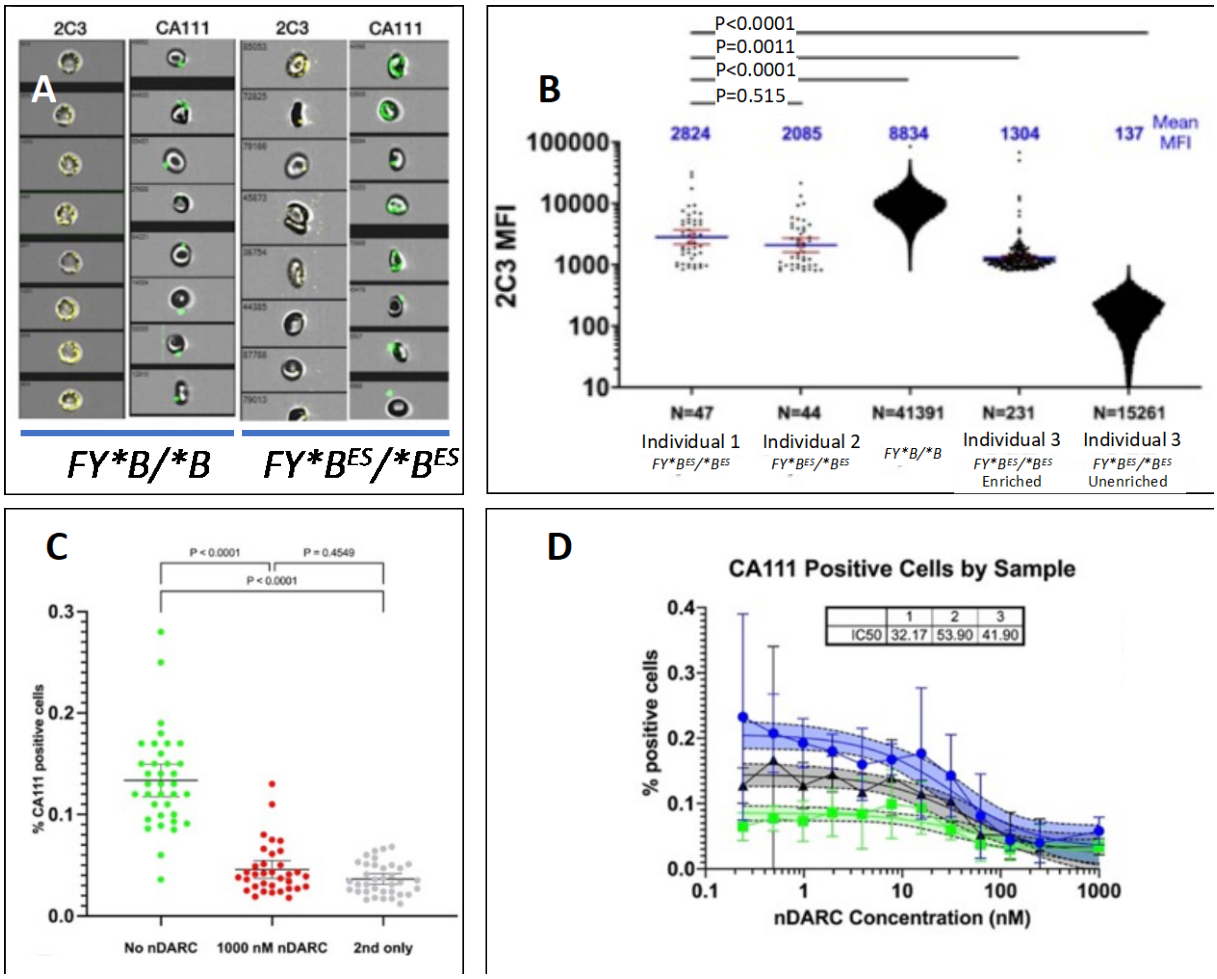

Figure S3: Quantification of DARC on *FY*B^{ES}/*B^{ES}* individuals and competition with nDARC related to Figure 1.

Panel S3A. IFC panel showing 2C3 or CA111 stained cells of a *FY*B/*B* and *FY*B^{ES}/*B^{ES}* individuals. The observed punctuated staining resembles similar images obtained by Kodippilli *et al* [S2].

Panel S3B. Cell-based intensity quantification of *FY*B^{ES}/*B^{ES}* and *FY*B/*B* cells. Displayed on the logarithmic y-axis is the 2C3 fluorescence intensity of each individual cell. Displayed below the graph are the number of individual cells that surpassed a threshold for 2C3 intensity >800 MFI.

Shown in blue are the mean intensity for those cells. A reticulocyte enrichment protocol was applied to one *FY*B*^{ES}*/*B*^{ES} sample and the number of positive cells exceeding the 800-threshold increased approximately tenfold (mean MFI enriched = 1,304; unenriched = 137). While all cells of a *FY*B/*B* individual surpassed this threshold, the mean intensity was approximately 3.6x higher compared to *FY*B*^{ES}*/*B*^{ES} individuals.

Panel S3C. CA111 binding in competition with nDARC - Merged data from three *FY*B*^{ES}*/*B*^{ES} individuals without nDARC (green) and 1,000 nM nDARC (red) in comparison to the background fluorescence of the 2nd antibody alone. P-values indicate that there is no statistical difference between secondary antibody and 1,000 nM DARC, suggesting complete blocking of CA111 binding when using 1,000 nM nDARC.

Panel S3D. Depleted RBCs from three *FY*B*^{ES}*/*B*^{ES} individuals probed by CA111 binding in the presence of increasing amounts of recombinant nDARC. The individual donor numbers correspond to those described in 3B. IC_{50} values in nanomolar for each person are shown in the inset. Whole blood of three *FY*B*^{ES}*/*B*^{ES} individuals (blue, grey, green) was passed through an NWF filter to deplete WBCs. Each blood sample was run 4x per nDARC competition concentration ranging from 1000 nM to 0.48 nM in 12 two-fold dilution series. Data was acquired by flow cytometry on an Attune flow cytometer equipped with a 96 well plate reader. The IC_{50} concentration required to reduce CA111 binding was calculated using a non-linear regression with four parameters and ranged from 32-54 nM (average 35 nM). Complete blocking of CA111 binding that is indistinguishable from the 2nd antibody stain alone was achieved with 1,000 nM nDARC present. Based on the 2C3 binding intensities to *FY*B*^{ES}*/*B*^{ES} cells we can derive that the amount of Fy protein on *FY*B*^{ES}*/*B*^{ES} RBCs is approximately 3.6x less compared to *FY*B/*B* RBCs and the frequency in depleted whole blood ranges between 0.2% and 0.08% of the total RBC population. Comparing cells in Panel S3A for 2C3 between *FY*B/*B* and *FY*B*^{ES}*/*B*^{ES} shows this clearly, while the staining for CA111 looks different, very likely because non-saturating conditions were achieved with *FY*B/*B* cells. The staining pattern for Fy on the surface of *FY*B*^{ES}*/*B*^{ES} individuals as well as

*FY*B/*B* individuals resembles what Kodippilli *et al.* in 2020 describe for *FY*B/*B* cells [S2].

5. Immunoprecipitation with CA111

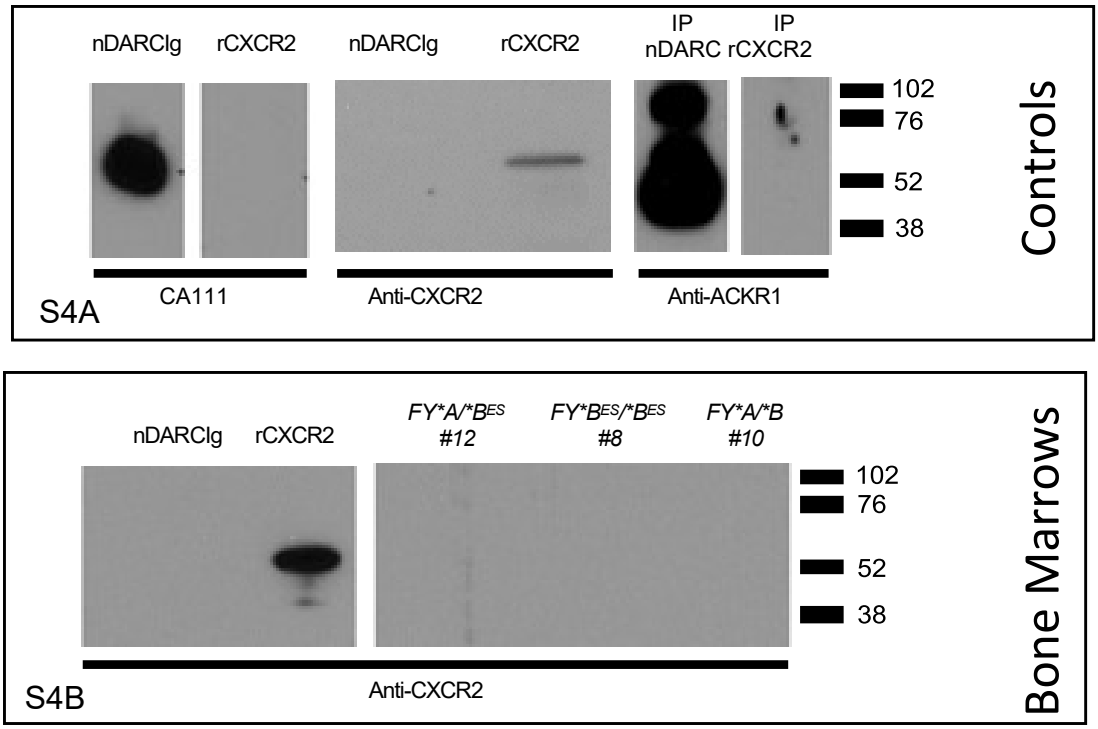

Figure S4. Binding specificity of CA111 to recombinant proteins nDARC and rCXCR2 related to Figure 4.

Panel S4A. Results show the characteristics of Fy-specific and CXCR2-specific antibody binding. CA111 binds to nDARCIg and does not bind to rCXCR2 (left). The anti-rCXCR2 antibody binds to rCXCR2 and not to nDARCIg (center). When CA111 was used to immunoprecipitate (IP) nDARCIg and rCXCR2, the resulting Western blot probed with a second Fy-specific antibody (anti-ACKR1) bound to nDARCIg and did not bind to rCXCR2 (right).

Panel S4B. CA111 was used to purify native Fy from bone marrow cells of donors characterized by different *FY* genotypes. The resulting Western blot was probed with anti- CXCR2. Controls in the two left lanes show that anti-CXCR2 antibody did not bind to nDARC, but did bind to rCXCR2. To confirm that CA111 does not pull down CXCR2 from human cells, we have tested the exact same samples as in Figure 5 of the main text (sorted CD45 negative cells from bone marrow samples). Results show that CA111 did not capture CXCR2 during immunoprecipitation as revealed by the absence of anti-CXCR2 signal in the three donor bone marrow samples (three right

lanes); results include bone marrow from both Fy-positive and Fy- negative people. See uncropped original films in section 7 (below).

6. Flow cytometric analysis of erythroid progenitor subpopulations in bone marrow

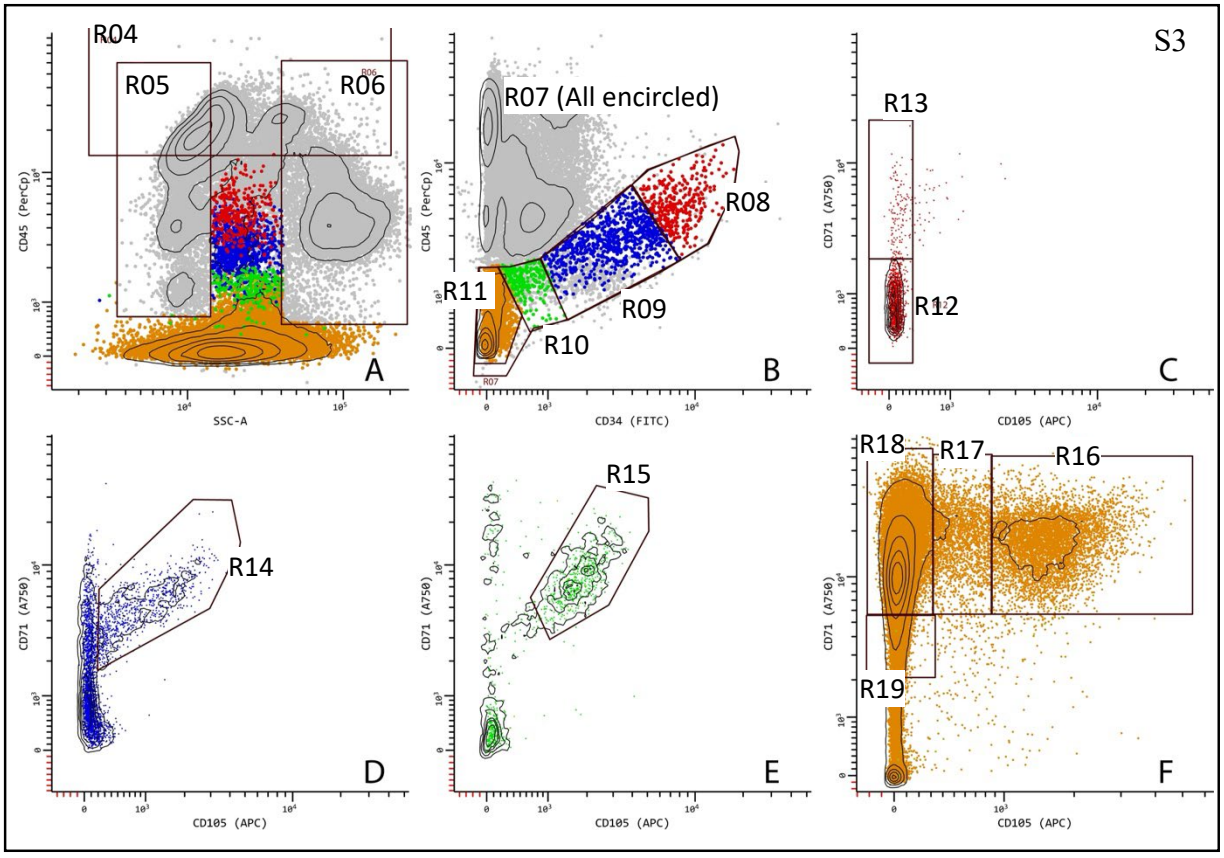

Figure S5. The gating strategy for sequential differentiation/maturation states of erythroid precursors in the bone marrow related to Figure 5.

The gating strategy follows the logic presented by Machherndal-Spandl *et al.* [S3], using ergodic principles [S4] and manual data classification that mimics probability state modeling [S5] and unsupervised seriation techniques [S6]. The idea that dynamic expression can be derived from static snapshots is well supported [S7],[S8]. First, single cell events are included with a primary gate on FSC-A vs FSC-H (not shown). Then, as shown in **panel S5A**, cells with lymphoid or mature myeloid granularity and CD45 expression are excluded (R04, R05, R06) with Boolean NOT gates. Next, shown in **panel S5B**, myeloid and erythroid precursors are included and subdivided as a function of decreasing CD34 and CD45 intensity (R08, R09, R10, R11; R07 is an all-inclusive gate

(R08, R09, R10, R11) used for monitoring but not data analysis). The CD34+/CD45+ precursors are further restricted based on the beginning expression of CD71 and CD105 (R12, R13, R14, R15, **panel S5C, S5D, S5E**). Finally, erythroid cells are defined by the correlated levels of CD105 and CD71 (R16, R17. R18, F19, **panel S5F**). From these regions, 8 sequential differentiation/maturation states are defined by Boolean logic as follows: *State 1*: R08 & R12 = CD34pos CD45pos CD105neg CD71neg ; *State 2*: R08 & R13 = CD34pos CD45pos CD105neg CD71pos ; *State 3*: R09 & R14 = CD34pos CD45pos CD105pos CD71pos ; *State 4*: R10 & R15 = CD34pos CD45mid CD105pos CD71pos ; *State 5*: R07 & R16 = CD34neg CD45neg CD105pos CD71pos ; *State 6*: R07 & R17 = CD34neg CD45neg CD105mid CD71pos ; *State 7*: R07 & R18 = CD34neg CD45neg CD105neg CD71pos ; *State 8*: R07 & R19 = CD34neg CD45neg CD105pos CD71mid. For those 8 states, R04, R05 and R06 were always excluded.

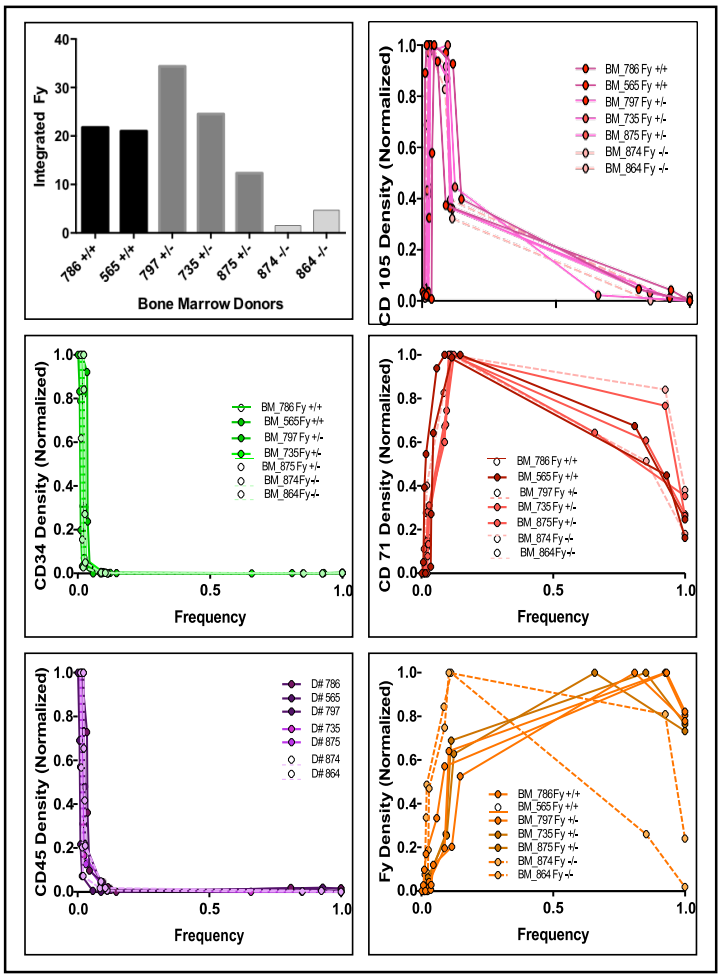

Figure S6. Frequency and time of each cell markers in immunophenotype state from the bone marrow related to Figure 5.

In orange, Fy density detected by CA111 is represented. All markers have the same kinetic of expression regardless of the Fy genotype except Fy expression in Fy-negative individual for which the time of expression is earlier (in term of immunophenotype state) than in Fy-positive donors.

7. Raw data for western blots

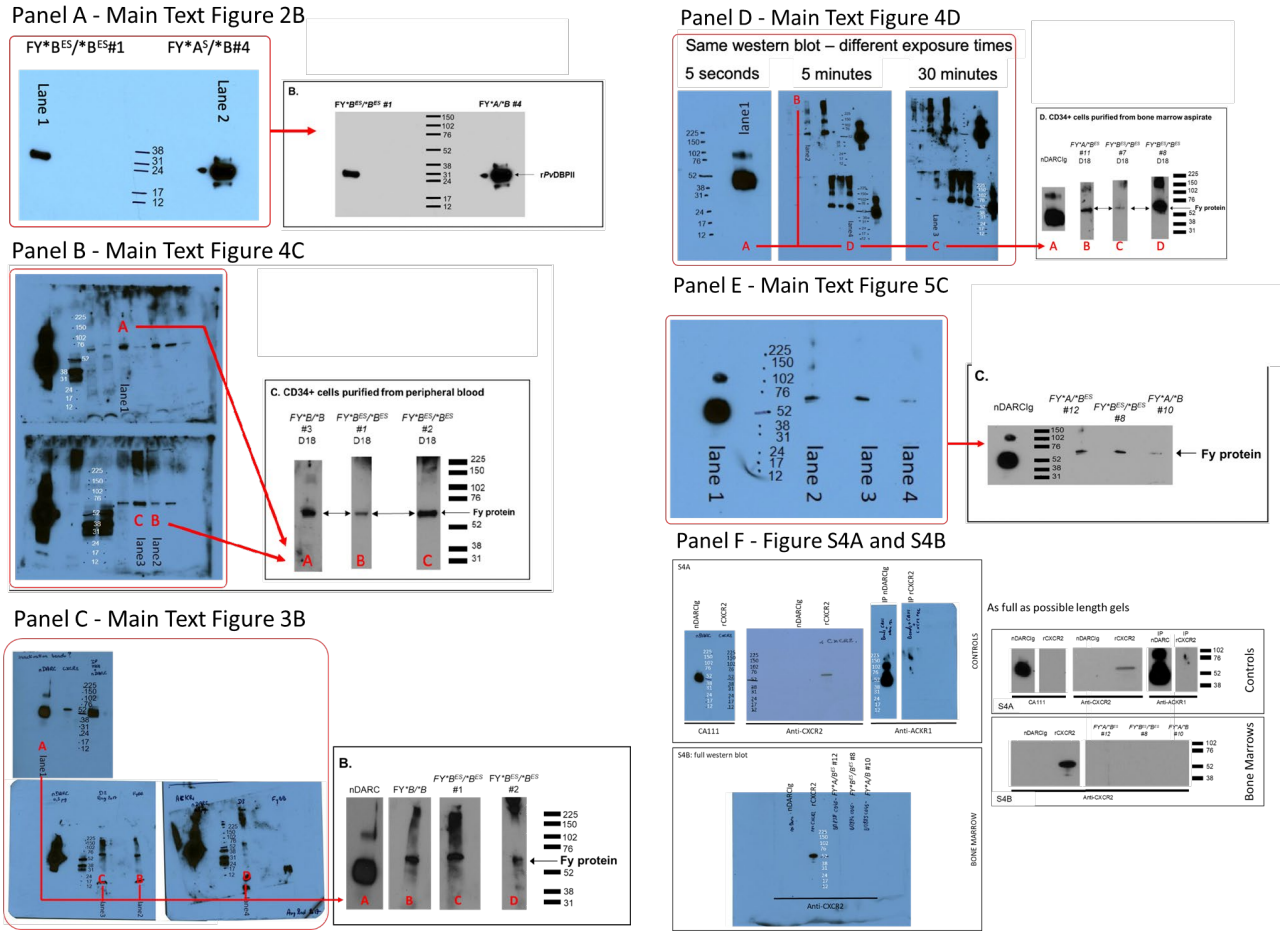

Figure S7: Raw data for western blots from Figures 2, 3, 4, 5

8. Imagestream

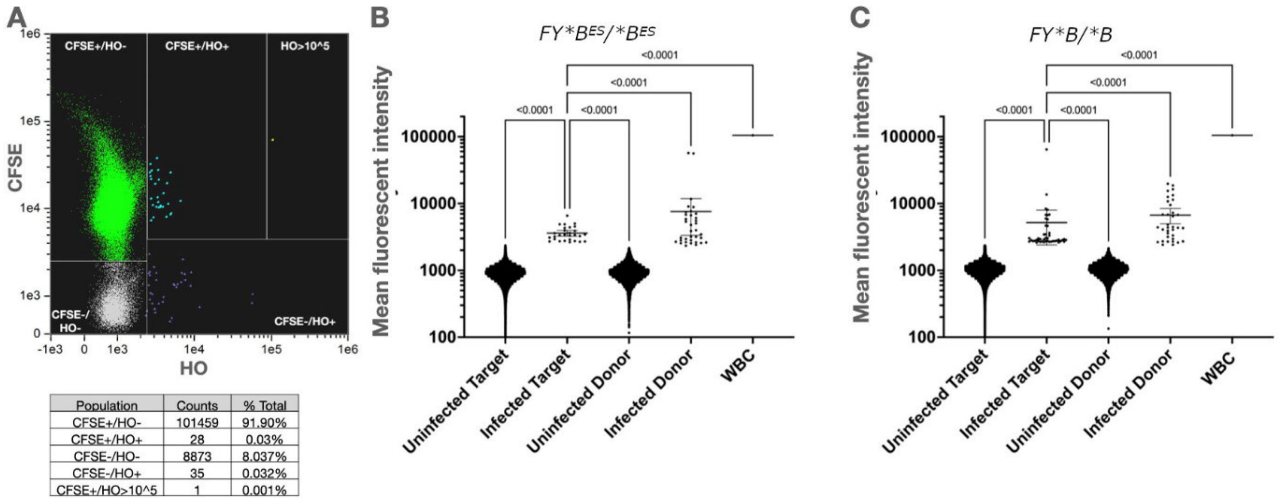

Population	Counts	% Total
CFSE+/HO-	101459	91.90%
CFSE+/HO+	28	0.03%
CFSE-/HO-	8873	8.037%
CFSE-/HO+	35	0.032%
CFSE+/HO>10^5	1	0.001%

Figure S8: Imagestream analysis separation of populations and statistical analysis of individual cells related to Figure 6.

Panel S8A. *FY*B*^{ES}*/*B*^{ES} invasion experiment (Sample A3, Part1). Populations are represented in different colors and enumerated in the Table S2 (below). The CFSE intensity of the invaded cells is indistinguishable from the target cell population (CFSE-labeled) but clearly distinguishable from the donor cell population (not CFSE labeled). Infected target cells can be clearly distinguished with statistical significance from either uninfected cells or white blood cells. Data shows 8,873 uninfected donor cells (grey; CFSE-HO-), 35 infected donor cells (dull blue; CFSE-HO+; one likely white blood cell with HO intensity >10^5), 101,459 uninfected target cells (green; CFSE+HO-), 28 infected target cells (cyan; CFSE-HO+).

Panel S8B. Statistical analysis of Imagestream plot (Panel S8A) of the different cell populations in the *FY*B*^{ES}*/*B*^{ES} invasion experiment (above).

Panel S8C. Statistical analysis of Imagestream data in the *FY*B/*B* invasion experiment *FY*B*^{ES}*/*B*^{ES} invasion experiment (Sample A1, Part1). Data shows 9,957 uninfected donor cells (grey; CFSE-HO-), 35 infected donor cells (dull blue; CFSE-HO+; one likely white blood cell with HO intensity >10^5), 86,613 uninfected target cells (green; CFSE+HO-), 79 infected target cells (cyan; CFSE-HO+).

Experiment	All Events (count)	Focused Events (count)	Single focused cells (count)	Infected Target cells CFSE+/HO+ (count)	Target cells / 100K single cells	Intensity Infected Target Cell, CFSE	Intensity Infected Target Cell, HO	WBC, HO >10^5 Intensity (count)	Intensity WBC, CFSE	Intensity WBC, HO
Background FY*B/*B	179945	116909	108308	32 *	30	19965.6	4016.2	1	104064.2	212234.7
A1 combined (10% seed)	1042897	678460	614771	350	57	23978.0	4101.2	1	206430.8	300343.0
B1 combined (10% seed)	864511	514785	460198	722	157	25150.2	3572.4	3	111322.4	356136.6
C1 Combined (20% seed)	535316	333622	312741	1010	323	21813.4	4278.6	12	75847.6	237454.1
Totals & Averages	**2442724**	**1526867**	**1387710**	**2082**	150	**23647.2**	**3984.1**	**16**	**131200.2**	**297977.9**
Background FY*B^{ES}/*B^{ES}	319567	214980	205972	28 *	14	26601.1	6773.6	5	22974.5	194437.7
A3 combined (10% seed)	706117	478360	442554	103	23	16839.5	3982.8	1	61319.0	104870.2
B3 combined (10% seed)	818519	474966	424397	326	77	15991.7	4077.8	5	99905.2	174218.0
C3 combined (20% seed)	651241	410126	379469	421	111	15138.6	4052.3	7	62687.2	160274.9
Totals & Averages	**2175877**	**1363452**	**1246420**	**850**	68	**15989.9**	**4037.6**	**13**	**74637.1**	**146454.4**

A= P. vivax isolate AMP2016.14
B= P. vivax isolate AMP2016.36
C= P. vivax isolate AMP2016.14

* False positive rate = False positives/(False positives+ Single cells)*100
False positive for Fy*B/*B = 0.029%
False positive rate for FY*BES/*ES = 0.014%

Table S2. Summary of all invasion experiments related to Figure 6.

The table summarizes all invasion experiments relevant to this (N=3; named “A”, “B” & “C”) with two different *P. vivax* isolates and varying amounts of infected donor population as seed either 10% or 20%.

Fig. S9: *FY*B^{ES}/*B^{ES} Pv*-infected cells related to Figure 6

Panel S9A. Experiment A3, part 1

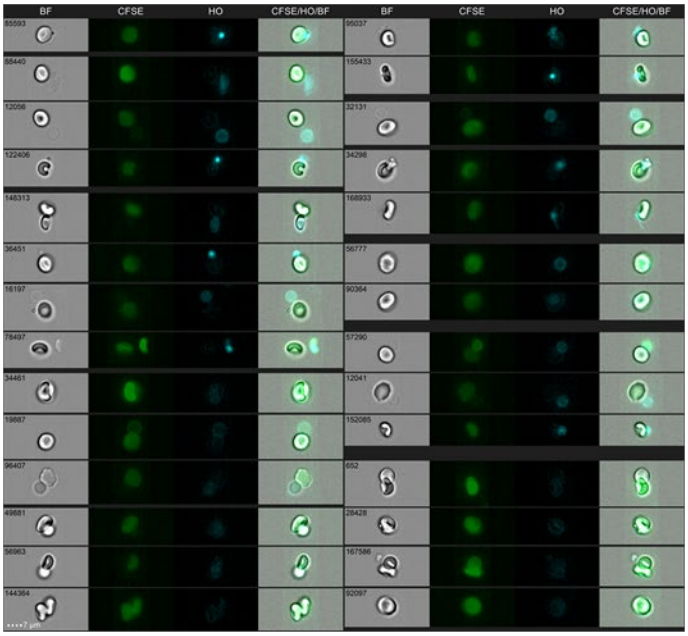

Panel S9C. Experiment A3, part 3

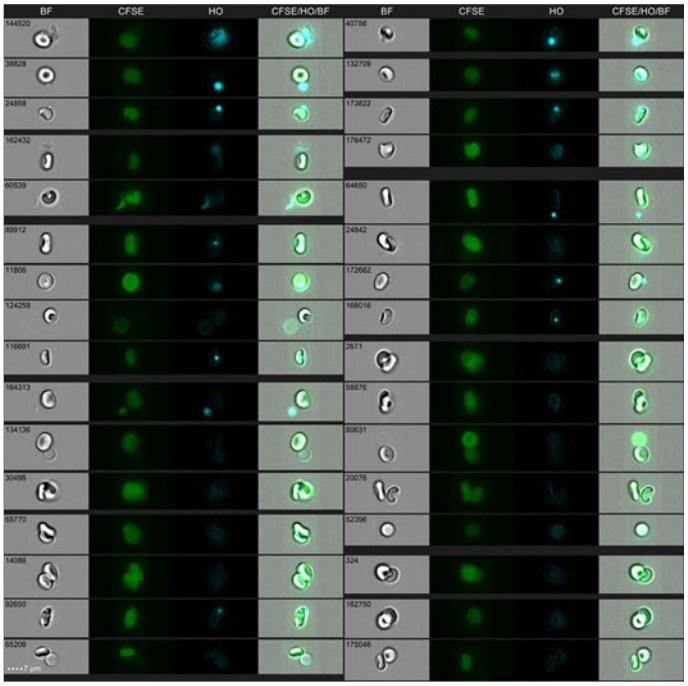

Panel S9B. Experiment A3, part 2

Panel S9D. Experiment A3, part 4

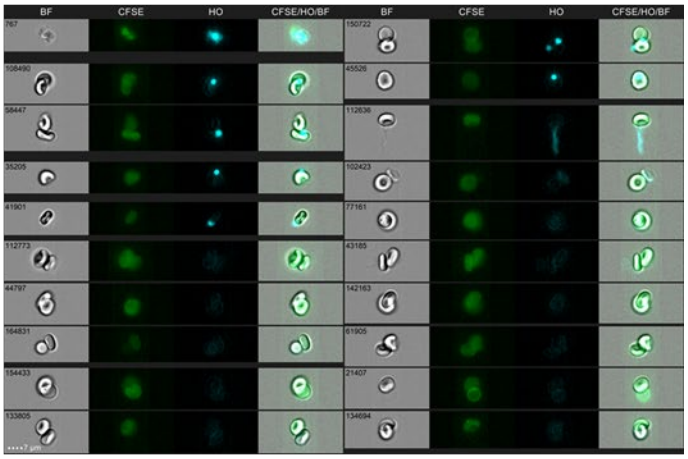

Panels A-D show 60x images taken with a brightfield channel, CFSE and HO channel and the composite merged image. Panels show composite results for *P. vivax* invasion of *FY*B^{ES}/*B^{ES}* target RBCs.

Fig. S10: *FY*B/*B Pv*-infected cells related to Figure 6

Panel S10A. Experiment A1, part 1

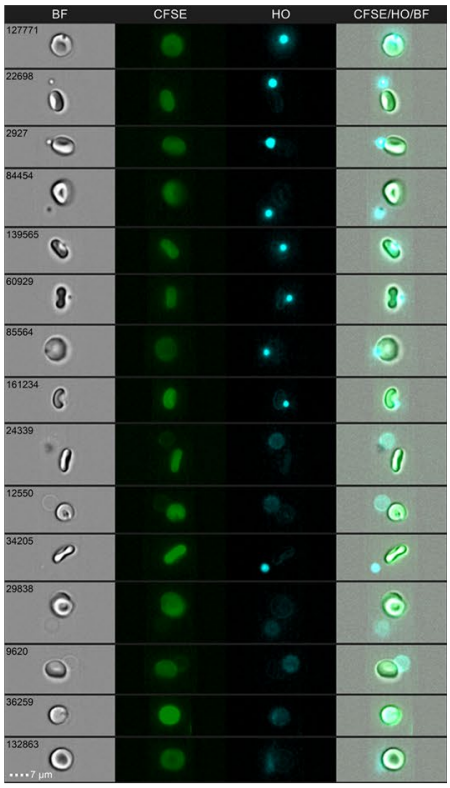

Panel S10C. Experiment A1, part 3

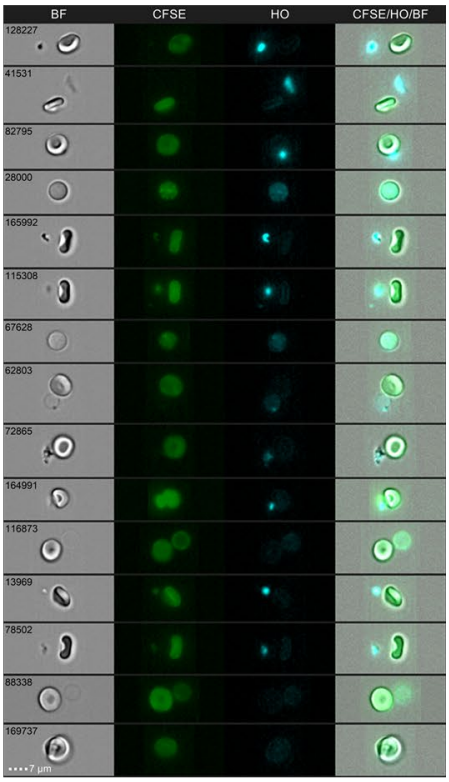

Panel S10B. Experiment A1, part 2

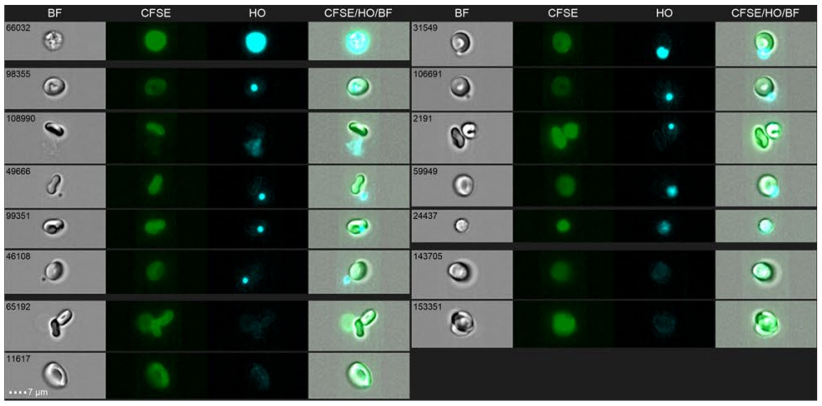

Panel S10D. Experiment A1, part 4

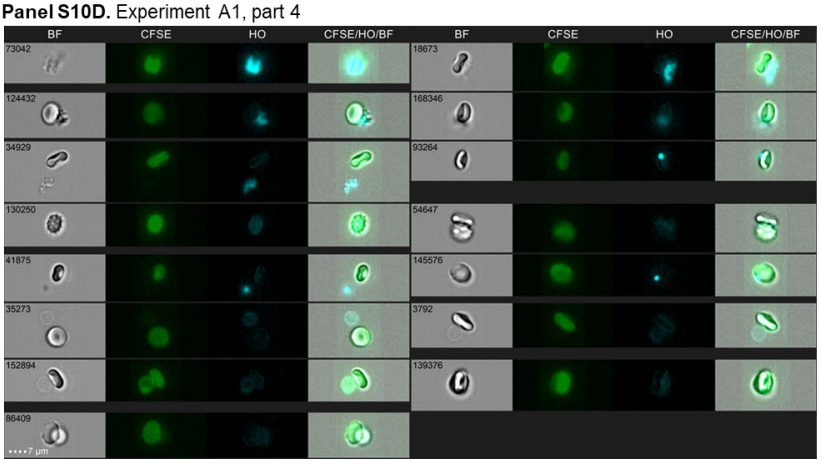

Panels A-D show 60x images taken with a bright field channel, CFSE and HO channel and the composite merged image. Panels show composite results for *P. vivax* invasion of *FY*B/*B* target RBCs.

Fig. S11: *FY*B/*B* donor cells related to Figure 6

Panel S11A. *FY*B/*B* donor infected cells

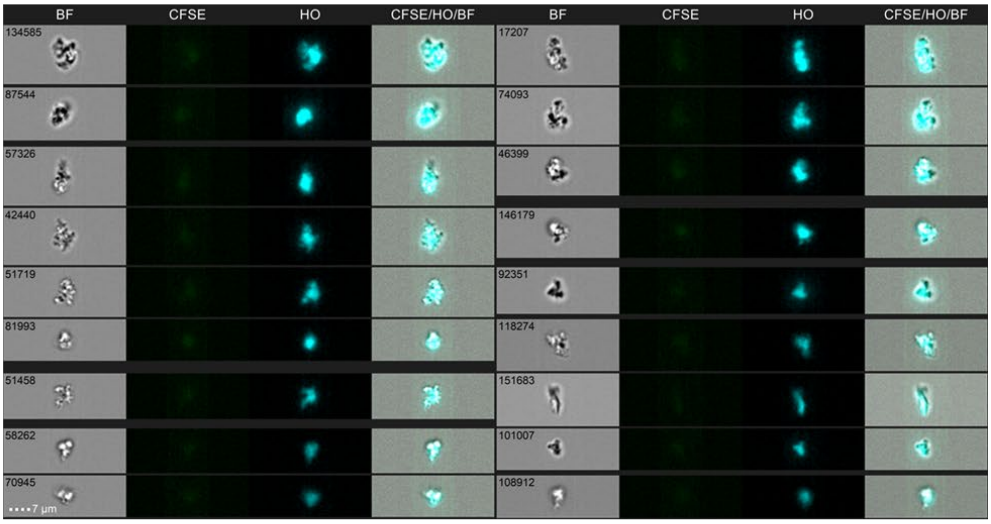

Panel S11B. *FY*B/*B* donor uninfected cells

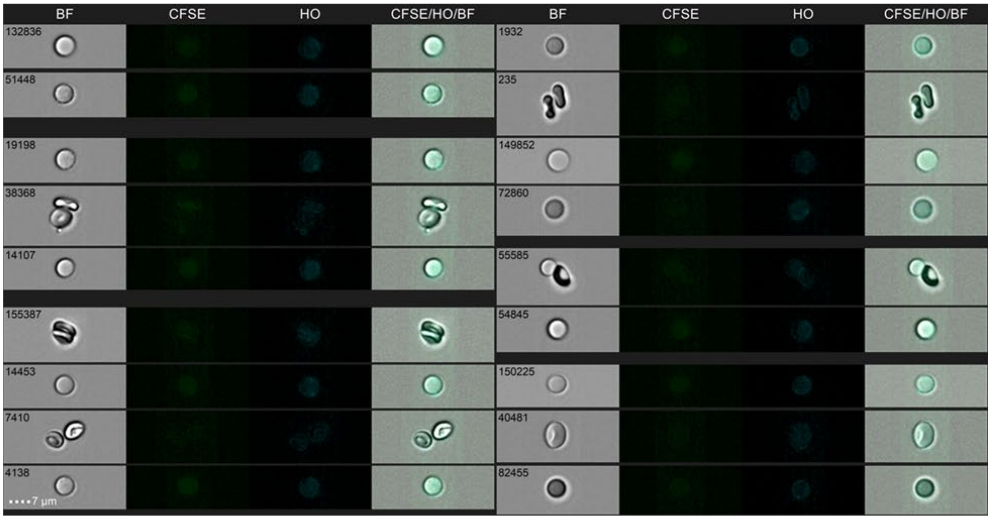

Panel S11C. *FY*B/*B* target uninfected cells

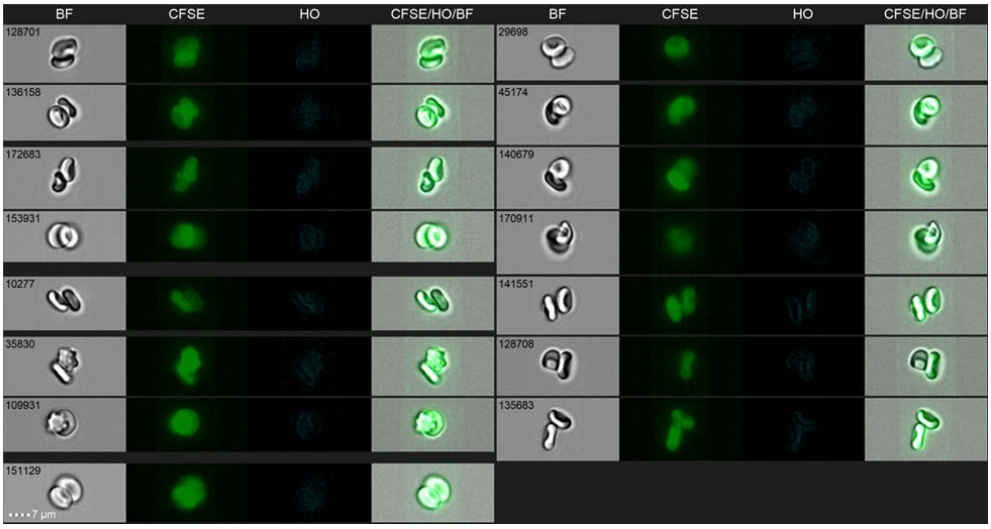

Panels A-D show 60x images taken with a brightfield channel, CFSE and HO channel and the composite merged image. Panels show composite results for *P. vivax* invasion controls of *FY*B/*B* target RBCs. Panel A: CFSE negative, HO positive; mostly ruptured RBCs with unreleased merozoites; Panel B: CFSE negative, HO negative; Panel C: CFSE positive, HO negative.

9. References

S1. Smolarek, D., Hattab, C., Hassanzadeh-Ghassabeh, G., Cochet, S., Gutiérrez, C., de Brevern, A.G., Udomsangpetch, R., Picot, J., Grodecka, M., Wasniowska, K., et al. (2010). A recombinant dromedary antibody fragment (VHH or nanobody) directed against human Duffy antigen receptor for chemokines. Cell Mol Life Sci 67, 3371–3387. 10.1007/s00018-010-0387-6.

S2. Kodippili, G.C., Giger, K., Putt, K.S., and Low, P.S. (2020). DARC, Glycophorin A, Band 3, and GLUT1 Diffusion in Erythrocytes: Insights into Membrane Complexes. Biophys J 119, 1749–1759. 10.1016/j.bpj.2020.09.012.

S3. Machherndl-Spandl, S., Suessner, S., Danzer, M., Proell, J., Gabriel, C., Lauf, J., Sylie, R., Klein, H.-U., Béné, M.C., Weltermann, A., et al. (2013). Molecular pathways of early CD105-positive erythroid cells as compared with CD34-positive common precursor cells by flow cytometric cell-sorting and gene expression profiling. Blood Cancer J 3, e100. 10.1038/bcj.2012.45.

S4. Wheeler, R.J. (2015). Analyzing the dynamics of cell cycle processes from fixed samples through ergodic principles. Mol Biol Cell 26, 3898–3903. 10.1091/mbc.E15-03-0151.

S5. Bagwell, C.B., Hill, B.L., Wood, B.L., Wallace, P.K., Alrazzak, M., Kelliher, A.S., and Preffer, F.I. (2015). Human B-cell and progenitor stages as determined by probability state modeling of multidimensional cytometry data. Cytometry B Clin Cytom 88, 214–226. 10.1002/cyto.b.21243.

S6. Saeys, Y., Van Gassen, S., and Lambrecht, B.N. (2016). Computational flow cytometry: helping to make sense of high-dimensional immunology data. Nat Rev Immunol 16, 449–462. 10.1038/nri.2016.56.

S7. Avva, J., Weis, M.C., Sramkoski, R.M., Sreenath, S.N., and Jacobberger, J.W. (2012). Dynamic expression profiles from static cytometry data: component fitting and conversion to relative, “same scale” values. PLoS One 7, e38275. 10.1371/journal.pone.0038275.

S8. Jacobberger, J.W., Avva, J., Sreenath, S.N., Weis, M.C., and Stefan, T. (2012). Dynamic epitope expression from static cytometry data: principles and reproducibility. PLoS One 7, e30870. 10.1371/journal.pone.0030870.